ACCOUNTS of chemical research

pubs.acs.org/accounts

Article

Development of PFAS-Free Locally Concentrated Ionic Liquid Electrolytes for High-Energy Lithium and Aluminum Metal Batteries

Xu Liu, Cheng Xu, Henry Adenusi, Yuping Wu,* and Stefano Passerini*

Cite This: *Acc. Chem. Res.* 2025, 58, 354−365

Read Online

ACCESS | Metrics & More | Article Recommendations

CONSPECTUS: Lithium-ion batteries (LIBs) based on graphite anodes are a widely used state-of-the-art battery technology, but their energy density is approaching theoretical limits, prompting interest in lithium-metal batteries (LMBs) that can achieve higher energy density. In addition, the limited availability of lithium reserves raises supply concerns; therefore, research on postlithium metal batteries is underway. A major issue with these metal anodes, including lithium, is dendritic formation and insufficient reversibility, which leads to safety risks due to short circuits and the use of flammable electrolytes.

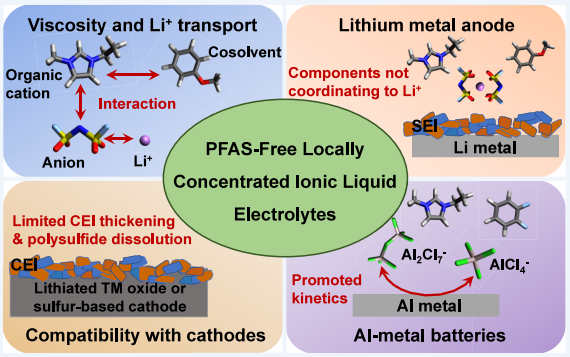

Ionic liquid electrolytes (ILEs), composed of metal salts and ionic liquids, offer a safer alternative due to their nonflammable nature and high thermal stability. Moreover, they can enable high Coulombic efficiency (CE) for lithium metal anodes (LMAs) and allow reversible stripping/plating of various post-lithium metals for battery application, e.g., aluminum metal batteries (AMBs). Despite these advantages, ILEs suffer from high viscosity, which impairs ion transport and wettability. To resolve these challenges, researchers have developed locally concentrated ionic liquid electrolytes (LCILEs) by adding low-viscosity nonsolvating cosolvents, e.g., hydrofluoroether, to ILEs. These cosolvents do not coordinate with cationic charge carriers, thereby reducing viscosity and improving ion transport without compromising the compatibility of electrolytes with metal anodes. However, due to the inherent difference of molecular organic solvents and ionic liquids full of charged species, the most used nonsolvating cosolvents, i.e., hydrofluoroether, are less effective for ILEs with respect to concentrated electrolytes based on conventional organic solvents. Moreover, hydrofluoroether contains environmentally problematic $-CF_3$ and/or $-CF_2$- groups, i.e., per- and polyfluoroalkyl substances (PFAS), with their use subject to restrictions.

In this Account, we provide an overview of the endeavors of our research group on the development of PFAS-free LCILEs for high-energy LMBs and AMBs. First, aromatic organic cations and aromatic less/nonfluorinated cosolvents are proposed to weaken the organic cation−anion interaction and strengthen the organic cation-cosolvent interaction, respectively. This is with consideration of the uncovered phase nanosegregation structure of LCILEs that effectively reduces the viscosity and promotes the Li^+ transport ability with respect to the conventional nonaromatic organic cations and highly fluorinated PFAS cosolvents. Then, the effect of electrolyte components that do not coordinate to Li^+, including organic cations and nonsolvating cosolvents, on the SEI composition and LMA reversibility is presented, which confirms the feasibility of reaching a high lithium stripping/plating CE up to 99.7% in the developed PFAS-free LCILEs. In the subsequent discussion on cathode compatibility, we present that in addition to $LiFePO_4$ with high cyclability but inferior energy density, nickel-rich layered oxide and sulfurized polyacrylonitrile (SPAN) can be employed to construct high-energy LMBs for PFAS-free LCILEs with different anodic stability. Additionally, the feasible application of the LCILE strategy to promote the kinetics of AMBs relying on a different anode chemistry is demonstrated. Lastly, future research directions with an emphasis on nonsolvating component optimization, electrolyte dynamics, and electrode/electrolyte interphase formation are provided.

KEY REFERENCES

- Liu, X.; Mariani, A.; Diemant, T.; Dong, X.; Su, P. H.; Passerini, S. Locally Concentrated Ionic Liquid Electrolytes Enabling Low-Temperature Lithium Metal Batteries. *Angew. Chem. Int. Ed.* **2023**, *62*, e202305840.[1] *Benefiting from the promoted Li^+transport and the preserved all-anion solvation sheath, PFAS-free locally*

Received: October 10, 2024
Revised: December 3, 2024
Accepted: December 3, 2024
Published: January 26, 2025

concentrated ionic liquid electrolytes with phase nanosegregation structure are reported to enable stable cycling of lithium metal batteries with 10 mg cm^{-2} $LiNi_{0.8}Co_{0.15}Al_{0.05}O_2$ cathodes at −20 °C.

- Liu, X.; Mariani, A.; Diemant, T.; Di Pietro, M. E.; Dong, X.; Su, P. H.; Mele, A.; Passerini, S. PFAS-Free Locally Concentrated Ionic Liquid Electrolytes for Lithium Metal Batteries. *ACS Energy Lett.* **2024**, *9*, 3049−3057.[2] *PFAS-free locally concentrated ionic liquid electrolytes employing a fluorine-free nonsolvating cosolvent are reported to enable Li plating/stripping Coulombic efficiency up to 99.71% and stable cycling of Li|| $LiFePO_4$ and Li||sulfurized-polyacrylonitrile batteries with 1.5-fold lithium metal excess for 400 and 350 cycles, respectively.*
- Liu, X.; Diemant, T.; Mariani, A.; Dong, X.; Di Pietro, M. E.; Mele, A.; Passerini, S. Locally Concentrated Ionic Liquid Electrolyte with Partially Solvating Diluent for Lithium/Sulfurized Polyacrylonitrile Batteries. *Adv. Mater.* **2022**, *34*, 2207155.[3] *This work reveals that the cathode electrolyte interphase derived mainly from organic cations and anions in PFAS-free locally concentrated ionic liquid electrolytes can suppress the dissolution of polysulfides and therefore enables stable cycling of high-energy sulfurized polyacrylonitrile cathodes.*
- Xu, C.; Diemant, T.; Mariani, A.; Di Pietro, M. E.; Mele, A.; Liu, X.; Passerini, S. Locally Concentrated Ionic Liquid Electrolytes for Wide-Temperature-Range Aluminum−Sulfur Batteries. *Angew. Chem. Int. Ed.* **2024**, *63*, e202318204.[4] *A PFAS-free locally concentrated ionic liquid electrolyte is reported, enabling aluminum−sulfur batteries with enhanced overall kinetics thanks to the nonsolvating cosolvent promoting the fluidity and ion transport without affecting the initial equilibrium of $AlCl_4^-$ and $Al_2Cl_7^-$ in the electrolyte.*

1. INTRODUCTION

Lithium-ion batteries (LIBs) as the state-of-the-art battery technology have been widely used in portable electronics and electric vehicles.[5] Nonetheless, the energy density of conventional LIBs relying on graphite anodes approaches the theoretical limit. This has led to the exploration of lithium-metal anodes (LMAs) with considerably higher specific capacities than graphite anodes for higher energy density batteries, i.e., lithium-metal batteries (LMBs).[6] At the same time, the low abundance and uneven distribution of lithium results in supply concerns owing to the elevated demand of lithium-based batteries.[7,8] Therefore, the investigation of post-lithium-metal batteries as complementary even as an alternative battery technology is underway.[9,10] The use of these metal anodes is limited by the challenges of reversibility and dendritic formation. The heat release accompanied by the interfacial side reactions and short circuit, together with the use of conventional flammable organic electrolytes, exacerbates the safety hazards of these high-energy-density batteries.[11]

In this context, ionic liquid electrolytes (ILEs) prepared via mixing metal salts and ionic liquids with bulky organic cations and anions as the solvent are an important class of electrolytes that can resolve these issues.[12] Due to their near-zero vapor pressure and high thermal stability, they are nonflammable, enhancing their safety profile for high-energy applications. Moreover, ILEs with rationally selected organic cations, anions, and salt concentration have been reported, enabling reversible stripping/plating of various metals for battery applications.[13−15] For instance, high Coulombic efficiency (CE) of lithium stripping/plating in ILEs above 99% has been reported.[16] ILEs and their analogues are the only electrolytes enabling reversible stripping/plating of aluminum at room temperature for aluminum metal batteries (AMBs).[16,17] On the other hand, the strong electrostatic force between cations and anions in ILEs increases their viscosity, which leads to poor wettability toward porous electrodes and sluggish ion transport.[18]

In recent years, the strategy of adding low-viscosity and nonsolvating cosolvents, e.g., hydrofluoroether, to concentrated electrolytes based on conventional organic solvents was used to address the aforementioned issues of ILEs, i.e., locally concentrated ionic liquid electrolytes (LCILEs).[19−21] Unlike the conventional solvating cosolvents, the nonsolvating cosolvent barely coordinates to the cationic charge carriers and therefore maintains the transference number and cationic charge carriers' solvation sheath in the parental ILEs. Consequently, the addition of these new cosolvents can decrease the viscosity and improve the ion transport without compromising the interfacial compatibility toward metal anodes. Nonetheless, due to the inherent difference of molecular organic solvents and ionic liquids full of charged species, the most commonly used nonsolvating cosolvents, i.e., hydrofluoroether, are less effective for ILEs.[21−23] Moreover, the hydrofluoroethers contain $-CF_3$ and/or $-CF_2$- groups, i.e., per- and polyfluoroalkyl substances (PFAS), also nicknamed "forever chemicals", and their use leads to environmental and occupational safety issues.[24,25] In fact, restrictions on the use of PFAS are now being considered worldwide. For instance, a proposal about restrictions on the manufacture, placing on the market, and use of PFAS in the European Union was submitted in January 2023 by authorities in Denmark, Germany, The Netherlands, Norway, and Sweden to the European Chemical Agency. On the other hand, these highly fluorinated groups were considered to be essential for the nonsolvating character of cosolvents and beneficial for the compatibility of LMAs.[22,26−28]

In this Account, we provide an overview of our endeavors on the development of several PFAS-free LCILEs for high-energy LMBs and AMBs. First, the selection of aromatic organic cations and less/nonfluorinated cosolvents with $\pi-\pi$ stacking interactions from the aspect of Li^+ transport and fluidity is presented. Subsequently, the strategy of promoting the reversibility of LMAs in PFAS-free LCILEs through optimization of electrolyte components that do not preferentially coordinate to Li^+ is discussed. Then, the compatibility of the developed PFAS-free LCILEs with high-energy-density cathodes for LMBs is discussed. In addition to LMBs, the feasible application of the LCILE strategy for Al−S batteries relying on a different anode chemistry is demonstrated. Lastly, a comment and perspective on future research directions is outlined.

The names and acronyms which will be used in this account for the organic cations, anions, and nonsolvating cosolvents of the LCILEs are shown in Table 1, along with their respective chemical structures shown in Figure 1.

https://doi.org/10.1021/acs.accounts.4c00653
Acc. Chem. Res. 2025, 58, 354−365

Table 1. Names and Acronyms for the Organic Cations, Anions, and Nonsolvating Cosolvents of the ILE and LCILEs

types	acronyms	names
organic cations	Pyr_{14}^+	*N*-butyl-*N*-methylpyrrolidinium cation
	$Emim^+$	1-ethyl-3-methylimidazolium cation
anions	FSI^-	bis(fluorosulfonyl)imide anion
cosolvents	BTFE	bis(2,2,2-trifluoroethyl) ether
	$BnOCH_3$	methoxybenzene
	BnF	fluorobenzene
	BnF_2	1,2-difluorobenzene
	$BnCF_3$	trifluoromethylbenzene
	$BnOCF_3$	trifluoromethoxybenzene

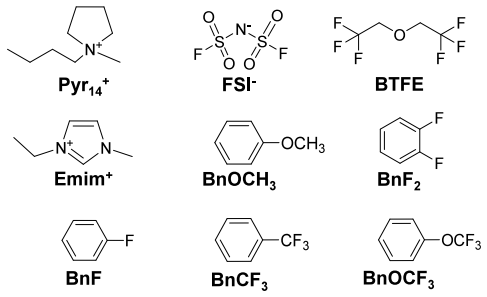

Figure 1. Chemical structures of the organic cations, anions, and nonsolvating cosolvents of the ILE and LCILEs.

2. ELECTROLYTE DESIGN PROMOTING LI^+ TRANSPORT AND FLUIDITY

Pyrrolidinium-based cations and hydrofluoroethers, as the most extensively studied organic cations for ILEs and nonsolvating cosolvents for locally concentrated electrolytes, respectively, are employed in the earliest exploration of LCILEs.[19,23,29,30] Although the LCILEs with an optimized molar ratio of the electrolyte components exhibited lower viscosity and promoted Li^+ transport ability with respect to the neat ILEs, their viscosity above 60 mPa·s at room temperature is inferior to that of locally concentrated electrolytes based on molecular organic solvents,[19,22,23,27,31] which also has a negative effect on the Li^+ transport. It needs to be mentioned that the high viscosity occurs for the LCILE whose formulation has been optimized with a focus on the Li^+ transport ability. Further addition of nonsolvating cosolvents and/or reduction of the lithium salt concentration can reduce the viscosity but will lead to worsened Li^+ transport ability. This lack of efficacy of LCILEs could be caused by the inherent difference of the molecular organic solvents and ionic liquids consisting of ions,[32−34] which thus necessitates further understanding of the microstructure and ion−ion/molecule interactions in LCILEs.

2.1. Local Heterogeneity of LCILEs

The prepared LCILEs appear as a macroscopical single phase, but a local heterogeneity is experimentally and computationally observed. Figure 2a displays the small-angle X-ray scattering (SAXS) patterns of $[LiFSI]_1[EmimFSI]_2[BnOCH_3]_6$, $[LiFSI]_1[EmimFSI]_2$, and $BnOCH_3$.[2] The latter two samples exhibit flat patterns at q values lower than 0.3 $Å^{-1}$, which

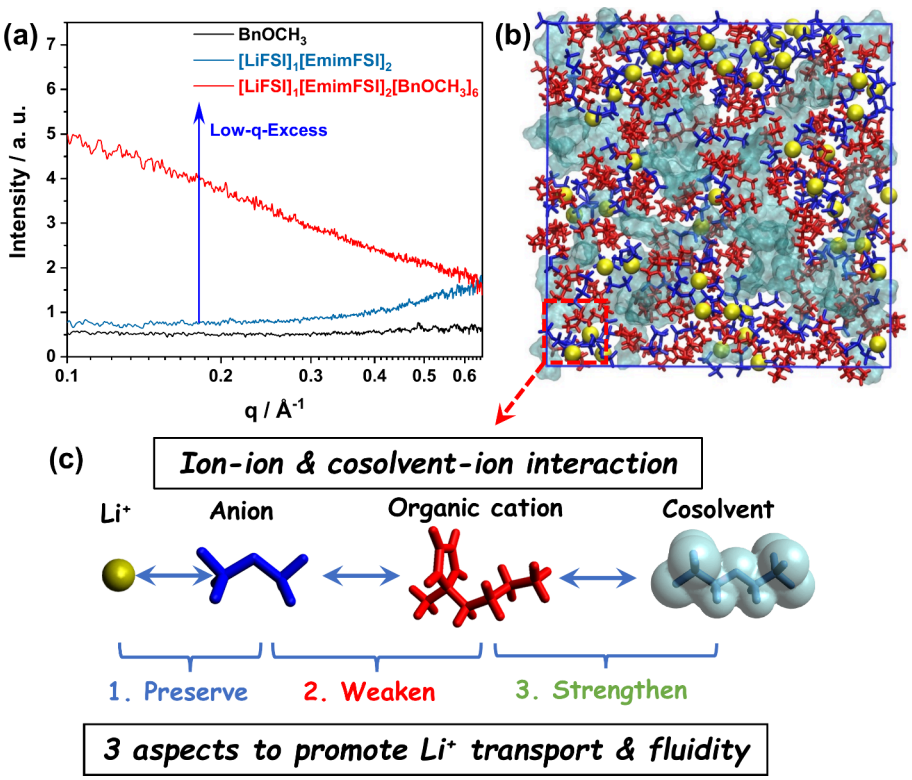

Figure 2. (a) SAXS patterns of a LCILE ($[LiFSI]_1[EmimFSI]_2[BnOCH_3]_6$) and the parental ILE ($[LiFSI]_1[EmimFSI]_2$) and cosolvent ($BnOCH_3$). Adapted from ref 2. Copyright 2024 American Chemical Society. (b) Snapshot of the MD simulation box of an LCILE ($[LiFSI]_1[Pyr_{14}FSI]_2[BTFE]_2$). Li^+, FSI^-, $Emim^+$, and BTFE are presented as yellow spheres, blue sticks, red sticks, and cyan clouds, respectively. Reproduced with permission from ref 36. Copyright 2021 Elsevier. (c) The ion−ion and cosolvent−ion interactions in LCILEs and the three approaches proposed to enhance their Li^+ transport.

https://doi.org/10.1021/acs.accounts.4c00653
Acc. Chem. Res. 2025, 58, 354−365

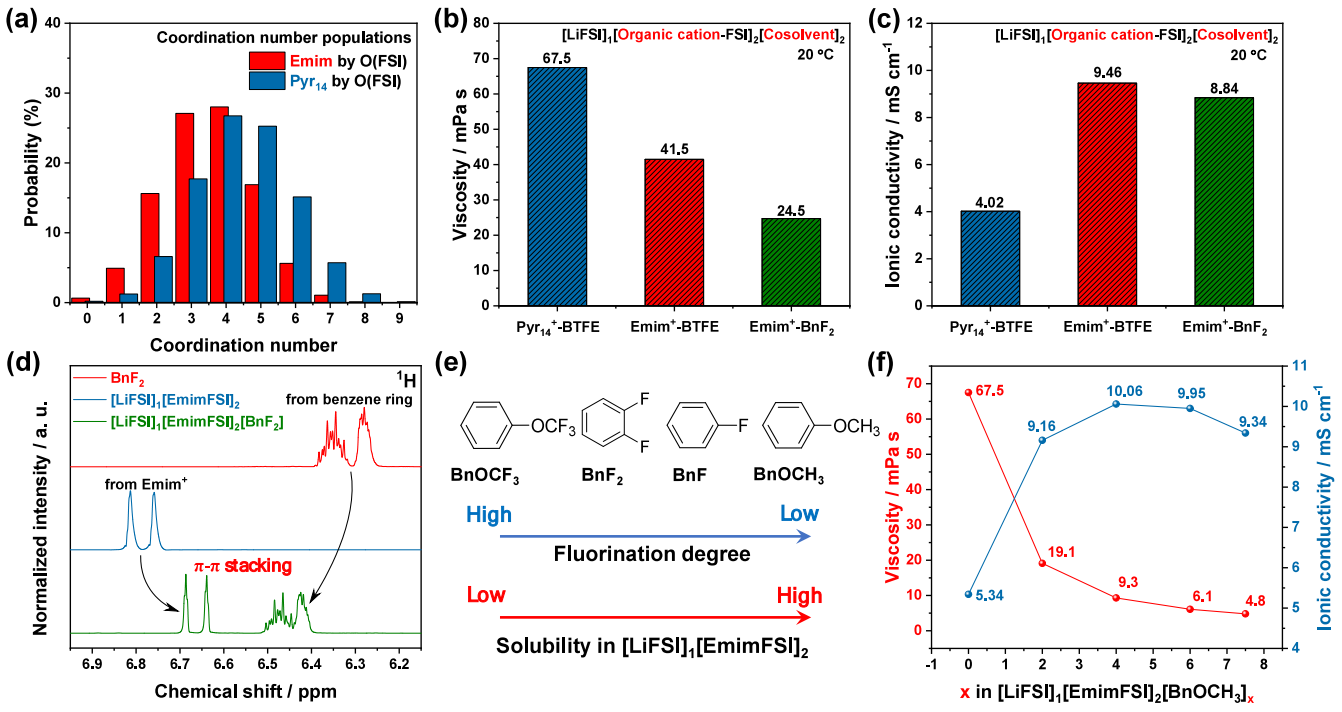

Figure 3. (a) Coordination number populations of $Emim^+/Pyr_{14}^+$ by oxygen from FSI^- obtained via MD simulation for $[LiFSI]_1[EmimFSI]_2[BTFE]_2$and $[LiFSI]_1[Pyr_{14}FSI]_2[BTFE]_2$. Adopted with permission from ref 36. Copyright 2021 Elsevier. (b) Viscosity and (c) ionic conductivity of $[LiFSI]_1[Pyr_{14}FSI]_2[BTFE]_2$, $[LiFSI]_1[EmimFSI]_2[BTFE]_2$, and $[LiFSI]_1[EmimFSI]_2[BnF_2]_2$ at 20 °C. The data of these two figures are from refs 36 and 42. (d) ^1H NMR spectra of BnF_2, $[LiFSI]_1[EmimFSI]_2$, and $[LiFSI]_1[EmimFSI]_2[BnF_2]_2$. Adapted from ref 42. Available under a CC-BY 4.0 license. Copyright 2022 The Authors. (e) Effect of fluorination degree of aromatic cosolvents on their solubility in $[LiFSI]_1[EmimFSI]_2$. (f) Viscosity and ionic conductivity of $[LiFSI]_1[EmimFSI]_2[BnOCH_3]_x$ (x = 0, 2, 4, 6, and 7.5) at 20 °C. Adapted from ref 2. Copyright 2024 American Chemical Society.

indicates that the ILE and cosolvent are homogeneous at scales larger than ∼20 Å. For the LCILE, its signal is much higher than the sum of the starting materials. This feature is known as Low-q-Excess and is the fingerprint of phase nanosegregation, meaning that the constituent phases of a macroscopically homogeneous mixture are separated at the nanoscale.[1,35] This phase nanosegregation can be computationally elucidated via molecular dynamics (MD) simulation.[1] For instance, Figure 2b displays the snapshots from MD simulations for $[LiFSI]_1[Pyr_{14}FSI]_2[BTFE]_2$, in which the yellow spheres, red sticks, blue sticks, and cyan clouds represent Li^+, Pyr_{14}^+, FSI^-, and BTFE, respectively.[36] As evidenced, most ions, including Li^+, FSI^-, and Pyr_{14}^+, aggregate to form ionic networks distinguished from the BTFE microdomains without Li^+, which corresponds well to the phase nanosegregation. A closer examination of the ionic networks reveals that Li^+ ions are directly coordinated by FSI^-, which is further surrounded by Pyr_{14}^+; BTFE interacts with Pyr_{14}^+ at the interface of the two microdomains (Figure 2c).

Among the interactions, the importance of the Li^+-FSI^- interaction present in all LiFSI-based electrolytes is widely known: preserving FSI^--rich Li^+ solvation is crucial to maintain the Li^+ transference number and the ability to generate robust anion-derived SEI rich in inorganic compounds on LMAs.[37−39] In contrast, the effect of organic cation−anion and organic cation−cosolvent interactions that uniquely exist in LCILEs is not well understood, which could contribute to the inferior fluidity and ion transport of LCILEs. The interaction between organic cations and anions is expected to affect the viscosity of LCILEs, which has been demonstrated in the extensive study of ionic liquids and ILEs.[29,40,41] The interaction between organic cations and cosolvents at the interface of the microdomains determines the miscibility of the cosolvent and the diluting effect.

2.2. Selection of Aromatic Organic Cations and Cosolvents

Considering the two unique interactions, our group replaces the conventional pyrrolidinium-based cations and hydrofluoroether cosolvents with aromatic ones, leading to further reduced viscosity and promoted Li^+ transport.

A comparative study of two LCILEs employing Pyr_{14}^+ or $Emim^+$ as the organic cation, i.e., $[LiFSI]_1[Pyr_{14}FSI]_2[BTFE]_2$ and $[LiFSI]_1[EmimFSI]_2[BTFE]_2$, revealed the beneficial effect of the aromatic cations.[36] Since the positively charged five-membered ring of $Emim^+$ obeys the Hückel rule, $Emim^+$ is conjugated and the positive charge is delocalized to the ring, which weakens the interactions toward FSI^-. MD simulations of these two electrolytes revealed that the average number of oxygen atoms from FSI^- coordinating to $Emim^+$ and Pyr_{14}^+ in their first solvation shell is 3.6 and 4.4, respectively (Figure 3a). As a result, the substitution of Pyr_{14}^+ with $Emim^+$ leads to an increase in ionic conductivity from 4.02 to 9.46 mS cm^{-1} and a decrease in viscosity from 67.5 to 41.5 mPa·s at 20 °C (Figure 3b, c). Moreover, the test of pulsed field gradient (PFG) nuclear magnetic resonance (NMR) indicates that the Li^+ self-diffusion coefficient is improved from 1.92×10^{-11} to 3.50×10^{-11} m^2 s^{-1} when $Emim^+$ is employed, and the Li^+ transference number in the electrolytes based on $Emim^+$ and Pyr_{14}^+ is 0.12 and 0.13, respectively. These results clearly demonstrate superior Li^+ transport in the $Emim^+$-based LCILE.

https://doi.org/10.1021/acs.accounts.4c00653
Acc. Chem. Res. 2025, 58, 354−365

In a further step, aromatic BnF_2 was adopted as an alternative of the hydrofluoroether cosolvent to construct LCILE.[42] It should be noted that BnF_2 is not a PFAS due to the absence of $-CF_2-$ and $-CF_3$ groups. Moreover, the cost of BnF_2 is much lower than that of the commonly used hydrofluoroether-based nonsolvating cosolvents, e.g., BTFE. With MD simulations and NMR, it was shown that aromatic $Emim^+$ with a positive charge interacts with aromatic BnF_2 rich in electrons via $\pi-\pi$ stacking (Figure 3d), which is generally stronger than the molecular interactions between $Emim^+$ and nonaromatic hydrofluoroether and therefore promotes the influence of the low-viscosity cosolvent on the fluidity of the LCILE.[42] At 20 °C, compared with $[LiFSI]_1[EmimFSI]_2[BTFE]_2$, $[LiFSI]_1[EmimFSI]_2[BnF_2]_2$ exhibits comparable ionic conductivity (8.84 mS cm^{-1}), Li^+ self-diffusion coefficient (3.50×10^{-11} m^2 s^{-1}), and Li^+ transference number (0.12) but significantly lower viscosity (24.7 mPa·s). Although further promotion is still required, this electrolyte has been able to allow stable cycling of LMBs employing 10 mg cm^{-2} $LiNi_{0.8}Mn_{0.1}Co_{0.1}O_2$ (NMC) cathodes at 20 °C with a discharge current density of 2 mA cm^{-2} (discussed in section 4.1). Moreover, the phase nanosegregation structure and the $\pi-\pi$ stacking interaction between $Emim^+$ and BnF_2 in this electrolyte are well preserved at subzero temperatures, which enables the operation of LMBs with 10 mg cm^{-2} $LiNi_{0.8}Co_{0.15}Al_{0.05}O_2$ (NCA) cathodes at −20 °C.[1]

It should be mentioned that such performance at room temperature and the operation of LMBs at subzero temperature is difficult to achieve with ILEs due to their high viscosity and sluggish Li^+ transport. These results also demonstrate that the aromatic organic cations and cosolvents are more suitable to construct LCILEs with lower viscosity and more robust Li^+ transport ability for more practical LMBs, compared with conventional pyrrolidinium-based cations and hydrofluoroether cosolvents.

2.3. Fluorination Degree of the Aromatic Cosolvents

The content of the nonsolvating cosolvents with significantly lower viscosity with respect to ILEs in the electrolyte directly affects the fluidity and the ion transport, while the fluorination degree of the aromatic cosolvent is shown to influence its solubility (Figure 3e). For $[LiFSI]_1[EmimFSI]_2[BnF_2]_x$, liquid−liquid phase separation occurs when x is increased from 2 to 3.[42] When $BnCF_3$ or $BnOCF_3$ with a higher fluorination degree than BnF_2 is employed as the cosolvent, an x value of 1 already leads to phase separation.[43] On the contrary, the use of BnF exhibiting a lower fluorine content than BnF_2 allows x to reach 3 without phase separation.[3] These phenomena can be explained by the effect of the fluorinated groups on the $\pi-\pi$ interactions between $Emim^+$ and the cosolvents. The increased degree of fluorination strengthens the electron withdrawing effect and reduces the negative charge density on the benzene ring, which weakens the $\pi-\pi$ interactions and decreases the solubility of the aromatic cosolvent. Similarly, the reduced degree of fluorination increases the solubility via strengthening the $\pi-\pi$ interactions. Therefore, a relatively low fluorination degree of the aromatic cosolvents is actually more suitable to construct LCILEs from the aspect of viscosity and Li^+ transport. The use of PFAS-based aromatic cosolvents with strong electron withdrawing groups, i.e., $-CF_2-$ and $-CF_3$, is likely to lead to a low solubility in ILEs. Notably, the significantly reduced solubility of the aromatic cosolvent with improved fluorination degree is not observed in locally concentrated electrolytes based on conventional organic solvents,[28,44,45] which reflects the effect of the functional interaction between organic cations and cosolvents in the LCILE.

These results also suggest that enhancing the negative charge on the benzene ring could promote $\pi-\pi$ interactions and increase the cosolvent solubility. In this context, fluorine-free $BnOCH_3$ with a resonance structure is adopted as a cosolvent to construct LCILEs.[2] The electron pair on the oxygen atom is delocalized through the resonance effect to the benzene ring, which decreases the coordination ability of the oxygen and increases the negative charge density on the benzene ring.[46] As a result, the x value of $[LiFSI]_1[EmimFSI]_2[BnOCH_3]_x$ can reach up to 7.5 without the phase separation, which is much higher than the fluorinated cosolvents, including the fluorinated aromatic cosolvents and hydrofluoroether.[2] For the electrolyte with the optimal x value, i.e., 6, the viscosity and ionic conductivity at 20 °C are 6.1 mPa·s and 9.95 mS cm^{-1}, respectively (Figure 3f). Due to the high content of the fluorine-free cosolvent, the fluorine content of the electrolyte is decreased from 12.13 for $[LiFSI]_1[EmimFSI]_2$ to 5.28 mol L^{-1}, which is lower than that in the 1 mol L^{-1} $LiPF_6$ electrolytes used for commercial LIBs. Additionally, the dilution decreased the mass fraction of LiFSI and EmimFSI in the electrolytes, which together with the low cost of $BnOCH_3$ makes the LCILEs more cost-effective than neat ILEs.

3. EFFECT OF NONSOLVATING ELECTROLYTE COMPONENTS ON THE LITHIUM METAL ANODE−SOLID ELECTROLYTE INTERPHASE

The reversibility of LMAs directly determines the lifetime of LMBs. An increased lithium metal reservoir to compensate for the inferior reversibility is feasible to prolong the lifespan of LMBs but weakens the energy density of the batteries. FSI^--based ILEs are known to enable dendrite-free cycling of LMAs with CEs up to 99%.[16,38,39] However, this character is mostly obtained at relatively low current density (≤0.5 mA cm^{-2}) and/or above room temperature.[16,39] Lithium dendrites are frequently observed upon lithium deposition in ILEs at 0.5−1.0 mA cm^{-2} and room temperature.[3,20,47] With the aid of the nonsolvating cosolvent, dendrite-free deposition of lithium metal at room temperature and enhanced CE of lithium stripping/plating are generally observed, which can be attributed to the improved Li^+ transport and the modified SEI.[48,49] Nonetheless, how the electrolyte composition affects the SEI generated on LMAs in LCILEs is not well understood, leading to difficulty in electrolyte design for more robust LMAs.

It is generally accepted that the solvation sheath of Li^+ has a significant influence on SEI formation. Consequently, manipulating an anion-rich Li^+ solvation to generate anion-derived, inorganic-rich SEI is a mainstream electrolyte strategy to promote the reversibility of LMAs.[50,51] However, the solvation sheath of Li^+ in ILEs and LCILEs is full of anions. In this context, our focus has shifted to the components that do not coordinate to Li^+, i.e., organic cations and nonsolvating cosolvents.

3.1. Organic Cations

Organic cations are an essential component of ionic liquids that affect the electrical double layer and SEI on electrodes in the study of ILEs.[52,53] For the study of LCILEs, various organic

https://doi.org/10.1021/acs.accounts.4c00653
Acc. Chem. Res. 2025, 58, 354−365

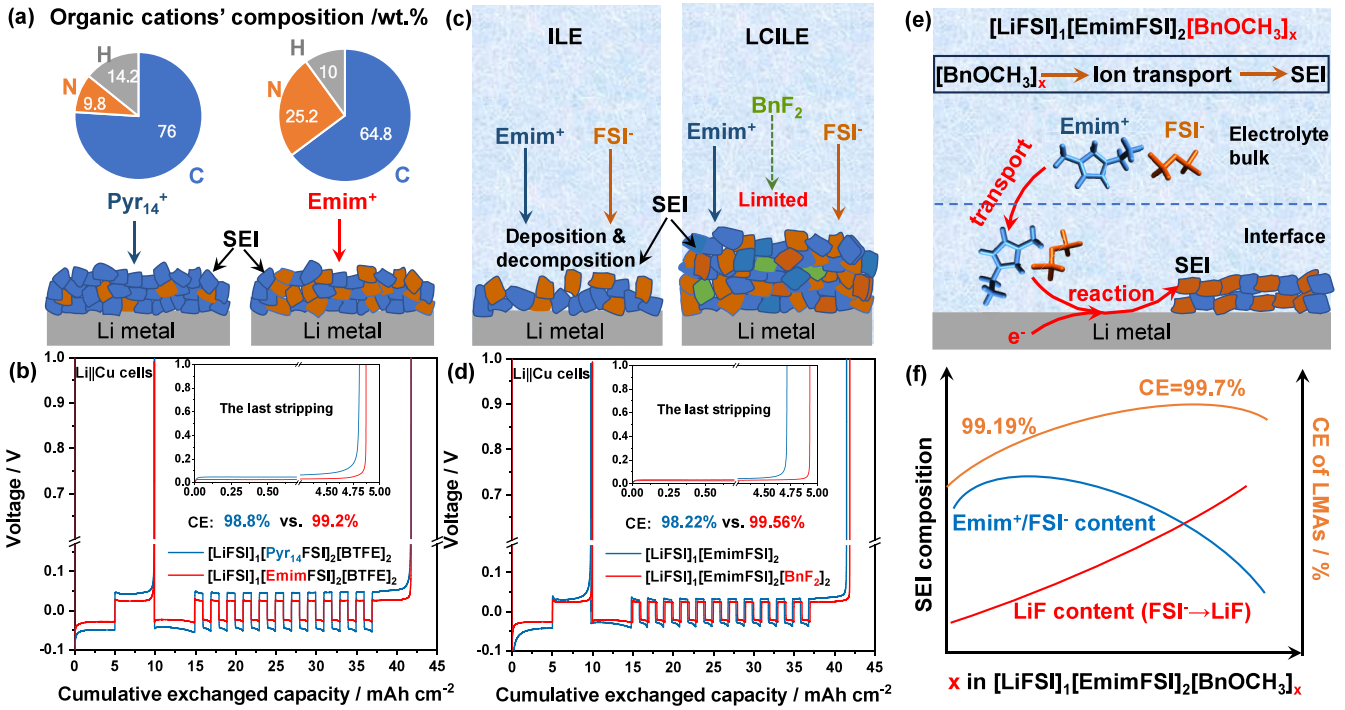

Figure 4. (a) Schematic illustration of the effect of $Emim^+$and Pyr_{14}^+ on the SEI generated on LMAs. (b) Voltage evolution of Li||Cu cells for the evaluation of lithium stripping/plating CE in LCILEs employing either $Emim^+$ or Pyr_{14}^+ as the organic cation. Adopted with permission from ref 36. Copyright 2021 Elsevier. (c) Schematic illustration of the effect of BnF_2 cosolvent added to $[LiFSI]_1[EmimFSI]_2$. (d) Voltage evolution of Li||Cu cells for the evaluation of lithium stripping and plating CE in $[LiFSI]_1[EmimFSI]_2$and $[LiFSI]_1[EmimFSI]_2[BnF_2]_2$. Adapted from ref 42. Available under a CC-BY 4.0 license. Copyright 2022 The Authors. (e, f) Schematic illustration of the effect of $BnOCH_3$ content in $[LiFSI]_1[EmimFSI]_2[BnF_2]_x$ on the SEI composition, CE of lithium stripping/plating, and their relation with the ion transport ability of electrolyte. Reproduced from ref 2.

cations have been employed,[19,20,23,48] but whether they participate the SEI formation and affect the electrochemical behavior of LMAs remains unclear. In the comparative study of $[LiFSI]_1[Pyr_{14}FSI]_2[BTFE]_2$ and $[LiFSI]_1[EmimFSI]_2[BTFE]_2$, it is revealed that both $Emim^+$ and Pyr_{14}^+ contribute to SEI formation.[36] Moreover, the higher nitrogen content of $Emim^+$ ($C_6H_{11}N_2^+$) with respect to Pyr_{14}^+ ($C_9H_{20}N^+$) increases the content of nitrogen-containing species in the SEI on LMAs (Figure 4a). The change on the SEI together with the enhanced Li^+ transport promote the CE of lithium stripping/plating from 98.8% in the Pyr_{14}^+-based electrolyte to 99.2% in the $Emim^+$-based electrolyte (Figure 4b).

3.2. Composition of Aromatic Cosolvents

The fluorinated groups of the cosolvent were considered to be beneficial for the compatibility of LMAs. This is because some of the cosolvents undergo defluorination, increasing the LiF content in the SEI,[28,45] while LiF as a good Li^+ conductor but an electronic insulator is a desired species for a robust SEI.[50] When the fluorinated cosolvent is replaced with a fluorine-free nonsolvating cosolvent for the concentrated electrolytes based on conventional organic solvent, the CE of LMAs is severely decreased.[50] For instance, the CE of LMAs in 3 M LiFSI in a mixture of 1,2-dimethoxyethane (DME) solvent and anisole cosolvent in a volume ratio of 1:2 only reaches 98.5%,[50] while CEs higher than 99.5% are commonly reported with locally concentrated electrolytes based on the same salt and solvent when fluorinated cosolvents are employed.[28,54,55]

Nonetheless, the X-ray photoelectron spectroscopy (XPS) study of the SEI on the lithium deposited and/or cycled in $[LiFSI]_1[EmimFSI]_2$, $[LiFSI]_1[EmimFSI]_2[BnF]_2$, and $[LiFSI]_1[EmimFSI]_2[BnF_2]_2$ indicates that the fluorine-related species of the SEI are mainly generated from the deposition and decomposition of FSI^-, and the contribution from the fluorinated cosolvent is limited.[3,42] Even though, the addition of BnF and BnF_2 manipulatesthe deposition and decomposition of $Emim^+$ and FSI^-, effectively promotes the CE of lithium stripping/plating.[3,42] For instance, BnF_2 cosolvent promotes the deposition of $Emim^+$ and FSI^- to generate a thicker SEI (Figure 4c), improving the CE from 98.2% for $[LiFSI]_1[EmimFSI]_2$ to 99.56% (Figure 4d).[56] It was observed that BnF and BnF_2 are also employed as the cosolvents for concentrated electrolytes based on conventional organic solvents, e.g., DME,[44] carbonate ester,[45] and phosphate ester.[57] However, their lithium stripping/plating CE is generally inferior to LCILEs,[44,45,57] especially with respect to $[LiFSI]_1[EmimFSI]_2[BnF]_2$ with a lithium stripping/plating CE of 99.72%.[3]

In addition, considering the overlapping of the signal of the C−F bond with C═O bond in C 1s XPS spectra and the S−F bond in F 1s XPS spectra, $BnCF_3$ and $BnOCF_3$ are employed as the cosolvents for $[LiFSI]_1[EmimFSI]_2$ to study the impact of the fluorinated cosolvent on the fluorine-containing species in the SEI.[43] The $-CF_3$ group is stable and usually does not fully decompose, and their much higher binding energy in the C 1s XPS spectra and F 1s spectra can minimize the interference of the other species.[58] Nonetheless, the signal of $-CF_3$ is not observed from the C 1s and F 1s spectra of the lithium cycled in $[LiFSI]_1[EmimFSI]_2[BnCF_3]_{0.55}$ and $[LiFSI]_1[EmimFSI]_2[BnOCF_3]_{0.55}$.[43]

https://doi.org/10.1021/acs.accounts.4c00653
Acc. Chem. Res. 2025, 58, 354−365

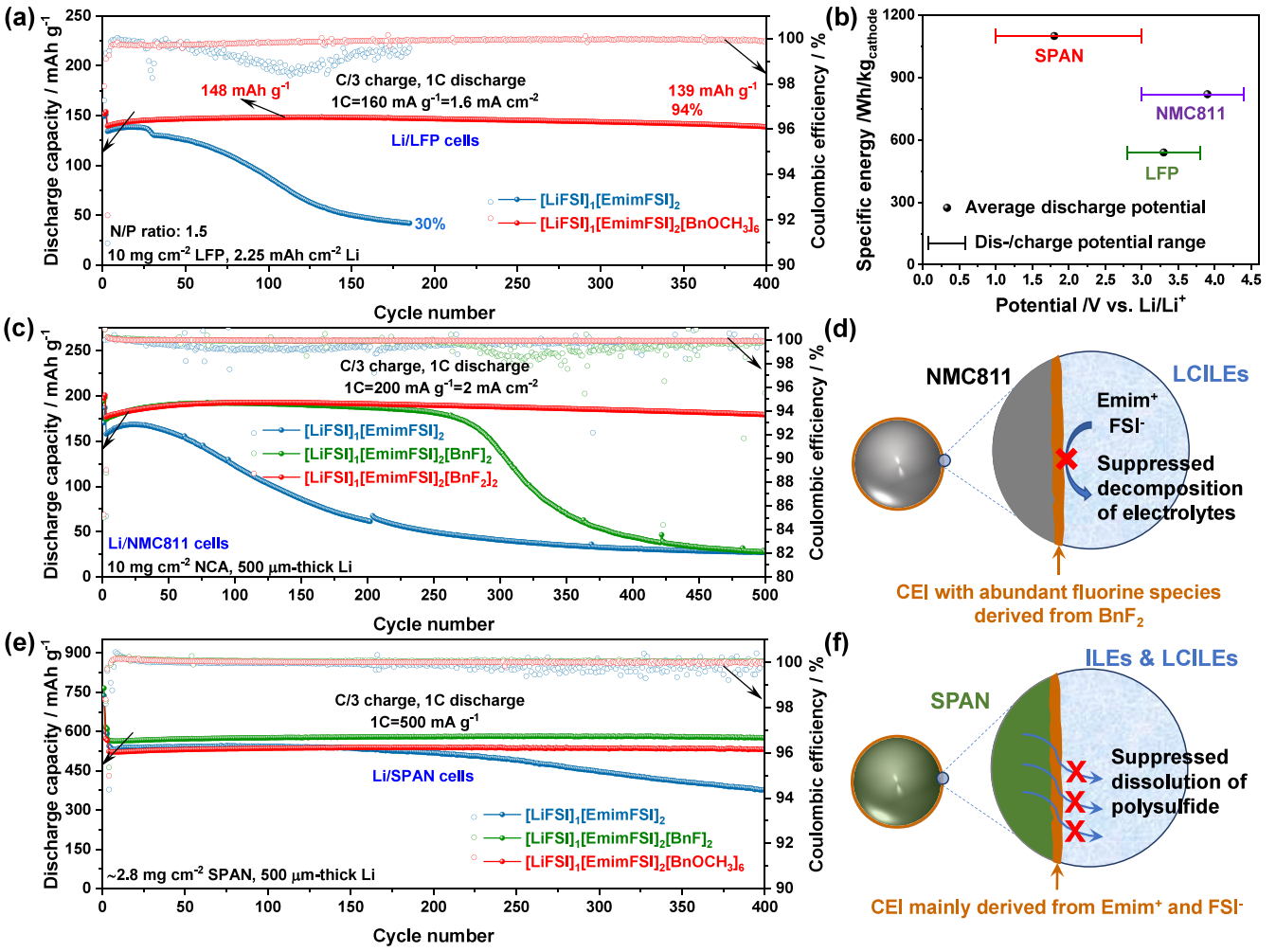

Figure 5. (a) Cyclability of Li||LFP cells employing $[LiFSI]_1[EmimFSI]_2$ or $[LiFSI]_1[EmimFSI]_2[BnOCH_3]_6$ as the electrolyte. Adapted from ref 2. Copyright 2024 American Chemical Society. (b) Average discharge potential, discharge/charge potential range, and specific energy of LFP, NMC811, and SPAN as cathode materials for LMBs. (c) Cyclability of Li||NMC811 cells employing $[LiFSI]_1[EmimFSI]_2$, $[LiFSI]_1[EmimFSI]_2[BnF]_2$, or $[LiFSI]_1[EmimFSI]_2[BnF_2]_2$ as the electrolyte. Adapted from ref 42. Available under a CC-BY 4.0 license. Copyright 2022 The Authors. (d) Schematic illustration of the promoted cyclability of NMC811 cathodes due to the mitigated electrolyte decomposition. (e) Cyclability of Li||SPAN cells employing $[LiFSI]_1[EmimFSI]_2$, $[LiFSI]_1[EmimFSI]_2[BnF]_2$, or $[LiFSI]_1[EmimFSI]_2[BnOCH_3]_6$as the electrolyte. Adapted from ref 2. Copyright 2024 American Chemical Society. Adapted from ref 3. Available under a CC-BY 4.0 license. Copyright 2022 The Authors. (f) Schematic illustration of the promoted cyclability of SPAN cathodes due to the mitigated polysulfide dissolution.

These results imply that the fluorinated groups of the nonsolvating cosolvent are not heavily involved in the SEI formation on LMAs in LCILEs and it could be feasible to reach a high reversibility of LMAs with nonfluorinated cosolvents. In fact, the CE of lithium stripping/plating in $[LiFSI]_1[EmimFSI]_2[BnOCH_3]_6$ is determined to be 99.7%,[2] which is much higher than the locally concentrated electrolytes employing $BnOCH_3$ cosolvent and DME solvent.[46]

3.3. Cosolvent Content

As previously introduced, the fluorinated cosolvents, including the hydrofluoroether and fluorinated aromatic compounds, exhibit limited solubility in ILEs. Due to the high solubility of $BnOCH_3$ in $[LiFSI]_1[EmimFSI]_2$, $[LiFSI]_1[EmimFSI]_2[BnOCH_3]_x$ (x = 0, 4, 6, and 7.5) were selected as the model electrolytes to study the effect of cosolvent content on the SEI composition and reversibility of LMAs, which reveals a correlation between ion transport and SEI composition (Figure 4e).[2] In general, the SEI generated in these electrolytes is mainly derived from $Emim^+$ and FSI^-, which suppresses the decomposition of $BnOCH_3$ and its involvement for SEI formation. As schematically illustrated in Figure 4f, the content of the species associated with the $Emim^+$ and FSI^- deposition in SEI exhibits a bell-shape evolution with increasing $BnOCH_3$ contents in the electrolyte, reaching the highest intensity when x is 4. This trend agrees with the ionic conductivity of the electrolytes (Figure 2f), implying a correlation between the SEI formation and the ions' transport. The correlation resides in the SEI formation being accompanied by the consumption of the ions at the electrolyte-electrode interface, which relies on their transport from the bulk electrolyte to the electrode interface (Figure 4e). Since the CE of lithium stripping/plating is promoted from 99.19% to 99.63% when x is increased from 0 to 4, the promoted deposition of $Emim^+$ and FSI^- is generally beneficial for a protective SEI. A similar phenomenon is also observed for $[LiFSI]_1[EmimFSI]_2[BnF_2]_2$. With a further increase of x, the reduced deposition of FSI^- is accompanied by its more

https://doi.org/10.1021/acs.accounts.4c00653
Acc. Chem. Res. 2025, 58, 354−365

pronounced reduction, as indicated by the higher intensity of the LiF in F 1s XPS spectra. Such a larger decomposition of FSI^- (to form LiF) can be considered as a consequence of the insufficient supply of ions at the electrode−electrolyte interface. These two opposite effects, i.e., reduced deposition of FSI^- and $Emim^+$ and the generation of LiF, arising from increasing anisole content control the reversibility of LMAs, and their balance when x is 6 leads to the highest lithium stripping/plating CE of 99.7%.

4. COMPATIBILITY WITH CATHODES FOR HIGH-ENERGY LITHIUM-METAL BATTERIES

The selection of cathode materials also plays an important role in determining the cyclability and energy density of the batteries. Due to the promoted fluidity, Li^+ transport, and LMA reversibility in the developed PFAS-free LCILEs, as well as the intrinsically high cyclability of $LiFePO_4$ (LFP), stable cycling of Li|LCILEs|LFP cells is expected. For instance, LMBs pairing 10 mg cm^{-2} LFP, 2.25 mAh cm^{-2} LMA, and $[LiFSI]_1[EmimFSI]_2[BnOCH_3]_6$ exhibited a capacity retention of 94% after 400 cycles at 20 °C (Figure 5a).[2] In contrast, the neat ILE, i.e., $[LiFSI]_1[EmimFSI]_2$, leads to a poor capacity retention of 30% after ∼200 cycles under the same conditions (Figure 5a).[2] The low cost and high cyclability of this cell make it a promising candidate for practical use. On the other hand, the LFP cathode limits the energy density of the batteries. From this aspect, efforts have been made toward the following two cathode materials with higher energy density compared to LFP (Figure 5b).

4.1. Nickel-Rich Layered Oxide

Nickel-rich layered oxides, e.g., $LiNi_xMn_yCo_{1-x-y}O_2$ ($x \geq 0.6$) and NCA, exhibiting higher energy density than LFP due to their higher specific capacity and average discharge potential are an important cathode competitor to LFP (Figure 5b).[59,60] Nonetheless, the higher operation potential and, particularly, the highly reactive Ni^{4+} generated upon charge result in a parasitic side reaction at the cathode electrolyte interface (CEI) and consequently poor cyclability.[61,62] Various ILEs have been reported to enable stable cycling of these cathodes, but the high stability is generally obtained at relatively low cathode loading, elevated temperature, and/or low current density.[39,63,64] Our study of the charge and discharge of NMC811 and NCA cathodes (10 mg cm^{-2}) at C/3 and 1C rate in $[LiFSI]_1[EmimFSI]_2$ at 20 °C revealed that the thickening of CEI derived from $Emim^+$ and FSI^- passivates the active material and therefore leads to fast capacity fading.[42,43] In contrast, when BnF and, particularly, BnF_2 are employed as the cosolvents to construct the PFAS-free LCILEs, the cyclability of NMC811 under the same test condition is significantly improved (Figure 5c).[42,43] The surface characterization of the NMC811 electrode cycled in $[LiFSI]_1[EmimFSI]_2[BnF_2]_2$ indicates that the decomposition of BnF_2 increases LiF and C−F species in CEI, which limits the deposition and decomposition of $Emim^+$ and FSI^- for the CEI thickening (Figure 5d). The inferior prolongation effect of the cyclability when BnF is employed as the cosolvent could be attributed to its lower fluorine content. $[LiFSI]_1[EmimFSI]_2[BnOCH_3]_6$ exhibiting a low anodic stability window of 3.9 V vs Li^+/Li is not compatible with the nickel-rich layered oxide cathodes.[2]

Therefore, an appropriate fluorination of the cosolvent is required for the design of LCILEs for this type of cathode material. Despite the presence of fluorine, the BnF_2-based LCILE is still free of PFAS. Due to its compatibility with both LMAs and NMC811 cathodes, the battery coupling 10 mg cm^{-2} NMC811 and 2 mAh cm^{-2} LMAs exhibits a decent capacity retention of 76% after 250 cycles at 20 °C.[42]

4.2. Sulfurized Polyacrylonitrile

Compared with $[LiFSI]_1[EmimFSI]_2[BnF_2]_2$, $[LiFSI]_1[EmimFSI]_2[BnF]_2$ and $[LiFSI]_1[EmimFSI]_2[BnOCH_3]_6$ exhibit higher compatibility toward LMAs but are less compatible with nickel-rich layer oxide cathodes. In this context, we proposed the use of sulfurized polyacrylonitrile (SPAN) as a cathode material for the LMBs employing these PFAS-free LCILEs. SPAN does not contain the catalytically reactive transition metals and exhibits a relatively low operational potential (usually 1.0−3.0 V vs Li^+/Li),[65] making it potentially compatible with the LCILEs with relatively inferior anodic stability. Meanwhile, a high specific capacity up to 600 mAh g^{-1} compensates for the low discharge potential and contributes to a remarkably high specific energy (Figure 5b).[65] It should be mentioned that elemental sulfur cathode usually suffers from poor cyclability in FSI^--based ILEs due to the dissolution of polysulfide, and the ILEs designed to enable more stable cycling of elemental sulfur cathodes are based on PFAS-based bis(trifluoromethanesulfonyl)imide anion.[66,67] Therefore, elemental sulfur was not selected to pair with the developed PFAS-free LCILEs. On the other hand, the cyclability of the SPAN cathode depends on whether the electrolyte is able to form a CEI that enables a solid−solid reaction mechanism with suppressed dissolution of polysulfide.[65,68] For instance, SPAN usually exhibits fast capacity fading in conventional ether-based electrolytes, e.g., 1 M LiFSI in DME, due to the lack of a protective CEI.[69]

$[LiFSI]_1[EmimFSI]_2$ and $[LiFSI]_1[EmimFSI]_2[BnF]_2$ were selected as model electrolytes to investigate the compatibility of ILEs and LCILEs toward SPAN cathodes.[3] It was shown that a similar CEI derived from the decomposition and deposition of $Emim^+$ and FSI^- is generated on SPAN cycled in the ILE and LCILE, suppressing the dissolution of polysulfide and enabling a stable cycling of SPAN cathodes (Figure 5e, f). Due to the higher reversibility of LMAs and faster Li^+ transport with respect to the ILE, the LCILE leads to more stable cycling and a high specific capacity of Li|SPAN cells, as displayed in Figure 5e. Since the cosolvent has a very limited effect on the CEI, SPAN could be compatible with other ILEs and LCILEs. For instance, the SPAN cathode also exhibits high cyclability in $[LiFSI]_1[EmimFSI]_2[BnOCH_3]_6$ with the generation of a CEI similarly derived from organic cations and anions (Figure 5e).[2] Benefiting from the high reversibility of both anodes and cathodes, a Li|$[LiFSI]_1[EmimFSI]_2[BnOCH_3]_6$|SPAN cell with 1.5-fold lithium excess exhibits a remarkable capacity retention of 90% after 350 cycles.[2]

5. APPLICATION FOR ALUMINUM-METAL BATTERIES

The impressive progress of LCILEs for LMBs has inspired their use for superior post-lithium-metal batteries.[70] Unlike alkali metal and alkaline-earth metals to realize the stripping/plating process via the redox couple of M^{n+}/M (M is the metal element, n = 1 for alkali metal and n = 2 for alkaline-earth metal), the stripping/plating of aluminum in AMBs relies on the conversion between chloroaluminate ions in the electrolytes, e.g., $AlCl_4^-$ and $Al_2Cl_7^-$, in the state-of-the-art electrolyte

https://doi.org/10.1021/acs.accounts.4c00653
Acc. Chem. Res. 2025, 58, 354−365

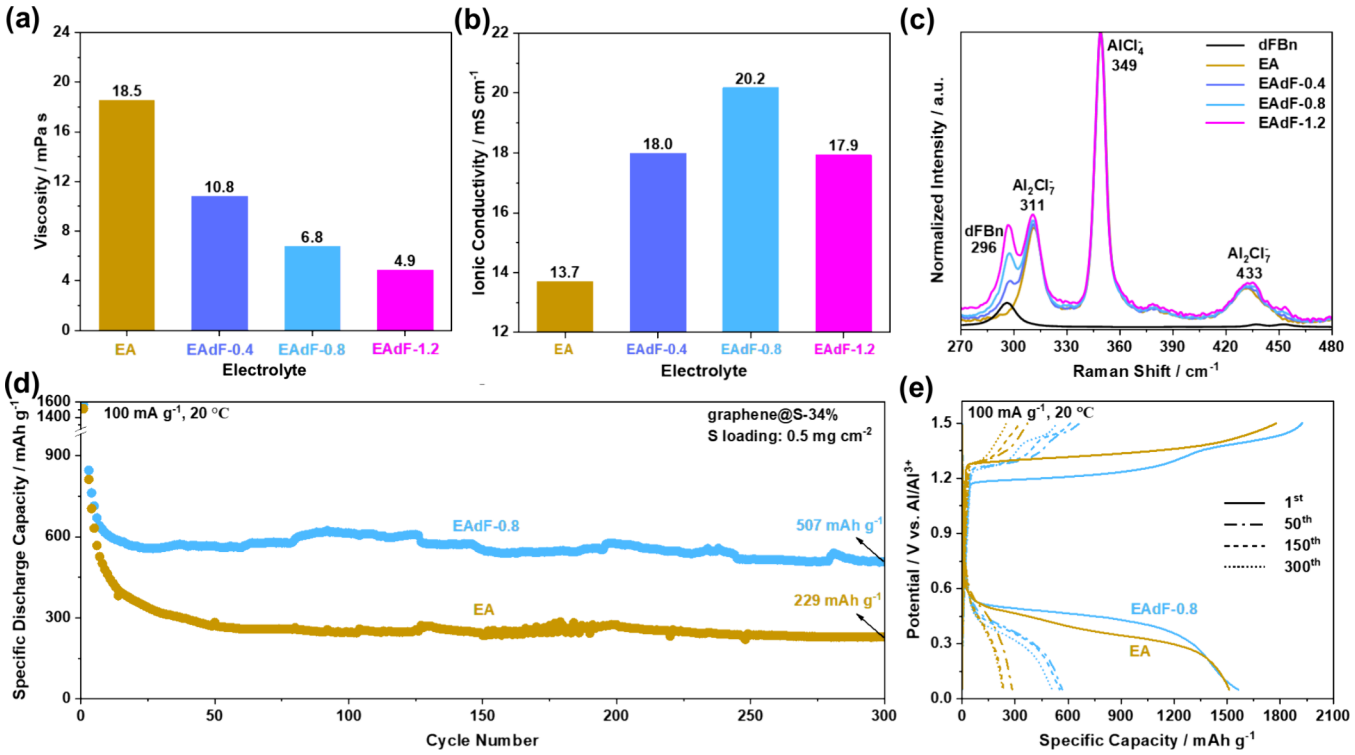

Figure 6. (a) Viscosity and (b) ionic conductivity of $[AlCl_3]_{1.3}[EmimCl]_1$(EA) and $[AlCl_3]_{1.3}[EmimCl]_1[BnF_2]_x$ (EAdF-*x*, *x* = 0.4, 0.8, and 1.2) at room temperature. (c) Raman spectra of EA, EAdF-*x*, and BnF_2. (d) Cyclability of Al−S batteries employing EA or EAdF-0.8 as the electrolyte and (e) corresponding discharge/charge profiles. Adapted from ref 4. Available under a CC-BY 4.0 license. Copyright 2022 The Authors.

$[AlCl_3]_{1.3}[EmimCl]_1$ for AMBs as described in the following equation:[16,17,71]

$$4Al_2Cl_7^- + 3e^- \leftrightarrow Al + 7AlCl_4^-$$

The equilibrium of $AlCl_4^-$ and $Al_2Cl_7^-$ is crucial for the stripping/plating of aluminum and is optimized via adjusting the molar ratio of $AlCl_3$ and EmimCl. Moreover, this type of electrolyte with strong Lewis acidity is highly reactive.[72] As a result, conventional solvating cosolvents and nonsolvating cosolvents with insufficient inertness cannot be applied, e.g., dimethyl carbonate and $BnOCH_3$.[73]

In this context, our group reported the use of BnF_2 as a cosolvent of $[AlCl_3]_{1.3}[EmimCl]_1$ to construct LCILE for aluminum metal batteries.[4] BnF_2 effectively decreases the viscosity and promotes the ionic conductivity without affecting the equilibrium between $AlCl_4^-$ and $Al_2Cl_7^-$ (Figure 6a−c), which preserves the reversible stripping/plating of aluminum and further promotes the overall kinetics of Al−S batteries. As a result, Al−S batteries employing LCILE sustain a remarkable capacity of 507 mAh g^{-1} after 300 cycles at 20 °C, while only 229 mAh g^{-1} is delivered with the neat ILE under the same condition (Figure 6d, e). This effect in Al−S batteries benefiting from the LCILE is also observed at temperatures deviating from room temperature, e.g., −20 and 40 °C.[4] In addition to ILEs, this strategy is proven to be effective for electrolytes based on deep eutectic liquids (also known as ionic liquid analogues), e.g., $[AlCl_3]_{1.3}[Urea]_1$, promoting the rate capability of Al-graphite batteries and the specific capacity of Al−S batteries at room temperature.[73]

6. SUMMARY AND OUTLOOK

Several PFAS-free LCILEs for high-energy LMBs and AMBs have been developed through step-by-step electrolyte optimization and identification of compatibility with relevant cathode materials. From the aspect of fluidity and Li^+ transport, aromatic organic cations and aromatic less/non-fluorinated cosolvents are more suitable than the conventional pyrrolidinium-based cations and highly fluorinated hydrofluoroether to construct LCILEs. The optimization of the components that do not favor coordination to Li^+ enables LMAs with a high CE up to 99.7% in the developed PFAS-free LCILEs. In addition to LFP, nickel-rich layered oxide and SPAN can be employed as cathode materials to construct high-energy LMBs, depending on the anodic stability of the PFAS-free LCILEs. In addition to LMBs, the LCILE strategy is also applicable for AMBs.

Optimization of organic cations and cosolvents is an important direction for the further development of LCILEs for LMBs due to their crucial roles in ion transport and electrolyte−electrode interphase (EEI) formation. For organic cations, the side chain of imidazolium-based cations can be functionalized to adjust the positive charge density and the composition. The exploration of the design of the cosolvent at the molecular level through the electron withdrawing effect of the fluorinated group, the resonance effect, and the steric effect is expected to modulate the solvating ability and electrochemical stability of cosolvents.

Understanding of the structure and ion−ion/ion-cosolvent interactions in the bulk of Li^+-based LCILEs has been attained, while their behavior on the electrode surface and in the electric field has yet to be explored. This information can guide the design of LCILEs with faster Li^+ transport in the bulk and the desolvation process at the electrode−electrolyte interface. In addition, the previous results indicate that the cosolvent can manipulate the contribution of organic cations and anions to the EEIs, and this effect changes with different cosolvents and

https://doi.org/10.1021/acs.accounts.4c00653
Acc. Chem. Res. 2025, 58, 354−365

different electrodes. Nonetheless, the mechanism behind this phenomenon is not clear. Further investigation on the mechanism of EEI formation at the molecular level is required to inform on the rational design of LCILEs. Apart from the conventional characterization of EEI, the analysis of the gas evolution and the decomposed species dissolved in the electrolytes can provide insightful information regarding the decomposition of the electrolyte components upon the formation of EEIs.

The decreased viscosity and superior ionic conductivity have been demonstrated to promote the kinetics of Al−S and Al−graphite batteries. Furthermore, although AMAs exhibit enhanced cyclability with the addition of nonsolvating cosolvents, the stripping/plating CE is far from 99%. For instance, the CE of aluminum stripping/plating is 80% and 88% in $[AlCl_3]_{1.3}[Urea]_1$ and $[AlCl_3]_{1.3}[Urea]_1[BnF_2]_{0.4}$, respectively. Therefore, improvement of the reversibility of AMAs is required. Unlike LMAs, the role of the SEI and its respective components on the reversibility of AMAs is unresolved. At this current stage, screening organic cations of ionic liquids, Lewis basic ligands of deep eutectic liquids, and nonsolvating cosolvents with different composition can elucidate the correlation between SEI composition and electrochemical performance.

AUTHOR INFORMATION

Corresponding Authors

Yuping Wu − *School of Energy and Environment & Z Energy Storage Center, Southeast University, 211189 Nanjing, China*; Email: wuyp@seu.edu.cn

Stefano Passerini − *Helmholtz Institute Ulm (HIU) Electrochemical Energy Storage, 89081 Ulm, Germany; Karlsruhe Institute of Technology (KIT), 76021 Karlsruhe, Germany; Center for Transport Technologies, Austrian Institute of Technology (AIT), 1020 Wien, Austria*; orcid.org/0000-0002-6606-5304; Email: stefano.passerini@kit.edu

Authors

Xu Liu − *School of Energy and Environment & Z Energy Storage Center, Southeast University, 211189 Nanjing, China; Helmholtz Institute Ulm (HIU) Electrochemical Energy Storage, 89081 Ulm, Germany; Karlsruhe Institute of Technology (KIT), 76021 Karlsruhe, Germany*; orcid.org/0000-0003-0532-316X

Cheng Xu − *Helmholtz Institute Ulm (HIU) Electrochemical Energy Storage, 89081 Ulm, Germany; Karlsruhe Institute of Technology (KIT), 76021 Karlsruhe, Germany*

Henry Adenusi − *Department of Science and Engineering of Matter, Environment and Urban Planning, Marche Polytechnic University, 60131 Ancona, Italy*

Complete contact information is available at: https://pubs.acs.org/10.1021/acs.accounts.4c00653

Author Contributions

Xu Liu: conceptualization (lead), writing-original draft (lead). **Cheng Xu**: writing-original draft (supporting), writing-review and editing (supporting). **Henry Adenusi:** writing-review and editing (supporting). **Yuping Wu**: supervision (lead), writing-review and editing (supporting). **Stefano Passerini**: conceptualization (equal), funding acquisition (lead), supervision (lead), writing-review and editing (lead).

Notes

The authors declare no competing financial interest.

ACKNOWLEDGMENTS

Financial support from the Helmholtz Association, the National Natural Science Foundation of China (No. 52131306), the Project on Carbon Emission Peak and Neutrality of Jiangsu Province (No. BE2022031-4), the Big Data Computing Center of Southeast University, and the Start-up Research Fund of Southeast University (4003002418) is acknowledged.

REFERENCES

(1) Liu, X.; Mariani, A.; Diemant, T.; Dong, X.; Su, P. H.; Passerini, S. Locally Concentrated Ionic Liquid Electrolytes Enabling Low-Temperature Lithium Metal Batteries. *Angew. Chem. Int. Ed.* **2023**, *62* (31), No. e202305840.

(2) Liu, X.; Mariani, A.; Diemant, T.; Di Pietro, M. E.; Dong, X.; Su, P. H.; Mele, A.; Passerini, S. PFAS-Free Locally Concentrated Ionic Liquid Electrolytes for Lithium Metal Batteries. *ACS Energy Lett.* **2024**, *9* (6), 3049−3057.

(3) Liu, X.; Diemant, T.; Mariani, A.; Dong, X.; Di Pietro, M. E.; Mele, A.; Passerini, S. Locally Concentrated Ionic Liquid Electrolyte with Partially Solvating Diluent for Lithium/Sulfurized Polyacrylonitrile Batteries. *Adv. Mater.* **2022**, *34* (49), 2207155.

(4) Xu, C.; Diemant, T.; Mariani, A.; Di Pietro, M. E.; Mele, A.; Liu, X.; Passerini, S. Locally Concentrated Ionic Liquid Electrolytes for Wide-Temperature-Range Aluminum-Sulfur Batteries. *Angew. Chem. Int. Ed.* **2024**, *63* (10), No. e202318204.

(5) Li, J.; Fleetwood, J.; Hawley, W. B.; Kays, W. From Materials to Cell: State-of-the-Art and Prospective Technologies for Lithium-Ion Battery Electrode Processing. *Chem. Rev.* **2022**, *122* (1), 903−956.

(6) Xu, W.; Wang, J.; Ding, F.; Chen, X.; Nasybulin, E.; Zhang, Y.; Zhang, J. G. Lithium Metal Anodes for Rechargeable Batteries. *Energy Environ. Sci.* **2014**, *7* (2), 513−537.

(7) Canepa, P.; Sai Gautam, G.; Hannah, D. C.; Malik, R.; Liu, M.; Gallagher, K. G.; Persson, K. A.; Ceder, G. Odyssey of Multivalent Cathode Materials: Open Questions and Future Challenges. *Chem. Rev.* **2017**, *117* (5), 4287−4341.

(8) Vaalma, C.; Buchholz, D.; Weil, M.; Passerini, S. A Cost and Resource Analysis of Sodium-Ion Batteries. *Nat. Rev. Mater.* **2018**, *3*, 18013.

(9) Tian, Y.; Zeng, G.; Rutt, A.; Shi, T.; Kim, H.; Wang, J.; Koettgen, J.; Sun, Y.; Ouyang, B.; Chen, T.; et al. Promises and Challenges of Next-Generation "Beyond Li-Ion" Batteries for Electric Vehicles and Grid Decarbonization. *Chem. Rev.* **2021**, *121* (3), 1623−1669.

(10) Zhang, H.; Qiao, L.; Kühnle, H.; Figgemeier, E.; Armand, M.; Eshetu, G. G. From Lithium to Emerging Mono- and Multivalent-Cation-Based Rechargeable Batteries: Non-Aqueous Organic Electrolyte and Interphase Perspectives. *Energy Environ. Sci.* **2023**, *16* (1), 11−52.

(11) Cheng, X. B.; Zhang, R.; Zhao, C. Z.; Zhang, Q. Toward Safe Lithium Metal Anode in Rechargeable Batteries: A Review. *Chem. Rev.* **2017**, *117*, 10403−10473.

(12) MacFarlane, D. R.; Forsyth, M.; Howlett, P. C.; Kar, M.; Passerini, S.; Pringle, J. M.; Ohno, H.; Watanabe, M.; Yan, F.; Zheng, W.; et al. Ionic Liquids and Their Solid-State Analogues as Materials for Energy Generation and Storage. *Nat. Rev. Mater.* **2016**, *1*, 15005.

(13) Rakov, D. A.; Chen, F.; Ferdousi, S. A.; Li, H.; Pathirana, T.; Simonov, A. N.; Howlett, P. C.; Atkin, R.; Forsyth, M. Engineering High-Energy-Density Sodium Battery Anodes for Improved Cycling with Superconcentrated Ionic-Liquid Electrolytes. *Nat. Mater.* **2020**, *19* (10), 1096−1101.

(14) Gao, X.; Mariani, A.; Jeong, S.; Liu, X.; Dou, X.; Ding, M.; Moretti, A.; Passerini, S. Prototype Rechargeable Magnesium Batteries Using Ionic Liquid Electrolytes. *J. Power Sources* **2019**, *423*, 52−59.

(15) Gao, X.; Liu, X.; Mariani, A.; Elia, G. A.; Lechner, M.; Streb, C.; Passerini, S. Alkoxy-Functionalized Ionic Liquid Electrolytes: Understanding Ionic Coordination of Calcium Ion Speciation for the Rational Design of Calcium Electrolytes. *Energy Environ. Sci.* **2020**, *13* (8), 2559−2569.
(16) Sun, H.; Zhu, G.; Zhu, Y.; Lin, M. C.; Chen, H.; Li, Y. Y.; Hung, W. H.; Zhou, B.; Wang, X.; Bai, Y.; et al. High-Safety and High-Energy-Density Lithium Metal Batteries in a Novel Ionic-Liquid Electrolyte. *Adv. Mater.* **2020**, *32* (26), 2001741.
(17) Lin, M. C.; Gong, M.; Lu, B.; Wu, Y.; Wang, D. Y.; Guan, M.; Angell, M.; Chen, C.; Yang, J.; Hwang, B. J.; et al. An Ultrafast Rechargeable Aluminium-Ion Battery. *Nature* **2015**, *520* (7547), 324−328.
(18) Pal, U.; Rakov, D.; Lu, B.; Sayahpour, B.; Chen, F.; Roy, B.; MacFarlane, D. R.; Armand, M.; Howlett, P. C.; Meng, Y. S.; et al. Interphase Control for High Performance Lithium Metal Batteries Using Ether Aided Ionic Liquid Electrolyte. *Energy Environ. Sci.* **2022**, *15* (5), 1907−1919.
(19) Lee, S.; Park, K.; Koo, B.; Park, C.; Jang, M.; Lee, H.; Lee, H. Safe, Stable Cycling of Lithium Metal Batteries with Low-Viscosity, Fire-Retardant Locally Concentrated Ionic Liquid Electrolytes. *Adv. Funct. Mater.* **2020**, *30* (35), 2003132.
(20) Cai, Y.; Zhang, Q.; Lu, Y.; Hao, Z.; Ni, Y.; Chen, J. An Ionic Liquid Electrolyte with Enhanced Li+ Transport Ability Enables Stable Li Deposition for High-Performance Li-O_2 Batteries. *Angew. Chem. Int. Ed.* **2021**, *60* (49), 25973−25980.
(21) Cao, X.; Jia, H.; Xu, W.; Zhang, J.-G. Review—Localized High-Concentration Electrolytes for Lithium Batteries. *J. Electrochem. Soc.* **2021**, *168* (1), No. 010522.
(22) Chen, S.; Zheng, J.; Mei, D.; Han, K. S.; Engelhard, M. H.; Zhao, W.; Xu, W.; Liu, J.; Zhang, J. G. High-Voltage Lithium-Metal Batteries Enabled by Localized High-Concentration Electrolytes. *Adv. Mater.* **2018**, *30* (21), 1706102.
(23) Liu, X.; Zarrabeitia, M.; Mariani, A.; Gao, X.; Schütz, H. M.; Fang, S.; Bizien, T.; Elia, G. A.; Passerini, S. Enhanced Li^+ Transport in Ionic Liquid-Based Electrolytes Aided by Fluorinated Ethers for Highly Efficient Lithium Metal Batteries with Improved Rate Capability. *Small Methods* **2021**, *5* (7), 2100168.
(24) Wang, Z.; Buser, A. M.; Cousins, I. T.; Demattio, S.; Drost, W.; Johansson, O.; Ohno, K.; Patlewicz, G.; Richard, A. M.; Walker, G. W.; et al. A New OECD Definition for Per- And Polyfluoroalkyl Substances. *Environ. Sci. Technol.* **2021**, *55*, 15575−15578.
(25) Flerlage, H.; Slootweg, J. C. Modern Chemistry Is Rubbish. *Nat. Rev. Chem.* **2023**, *7*, 593−594.
(26) Ren, X.; Chen, S.; Lee, H.; Mei, D.; Engelhard, M. H.; Burton, S. D.; Zhao, W.; Zheng, J.; Li, Q.; Ding, M. S.; et al. Localized High-Concentration Sulfone Electrolytes for High-Efficiency Lithium-Metal Batteries. *Chem.* **2018**, *4* (8), 1877−1892.
(27) Chen, S.; Zheng, J.; Yu, L.; Ren, X.; Engelhard, M. H.; Niu, C.; Lee, H.; Xu, W.; Xiao, J.; Liu, J.; et al. High-Efficiency Lithium Metal Batteries with Fire-Retardant Electrolytes. *Joule* **2018**, *2* (8), 1548−1558.
(28) Zhu, C.; Sun, C.; Li, R.; Weng, S.; Fan, L.; Wang, X.; Chen, L.; Noked, M.; Fan, X. Anion-Diluent Pairing for Stable High-Energy Li Metal Batteries. *ACS Energy Lett.* **2022**, *7* (4), 1338−1347.
(29) Elia, G. A.; Ulissi, U.; Jeong, S.; Passerini, S.; Hassoun, J. Exceptional Long-Life Performance of Lithium-Ion Batteries Using Ionic Liquid-Based Electrolytes. *Energy Environ. Sci.* **2016**, *9* (10), 3210−3220.
(30) Xu, T.; Qin, J.; Liu, Y.; Lan, Q.; Zhao, Y.; Song, Z.; Zhan, H. Diluted Ionic Liquid Electrolyte-Assisted Stable Cycling of Small Molecular Organics. *ChemElectroChem.* **2021**, *8* (23), 4625−4632.
(31) Ren, X.; Zou, L.; Cao, X.; Engelhard, M. H.; Liu, W.; Burton, S. D.; Lee, H.; Niu, C.; Matthews, B. E.; Zhu, Z.; et al. Enabling High-Voltage Lithium-Metal Batteries under Practical Conditions. *Joule* **2019**, *3* (7), 1662−1676.
(32) Li, L.; Cheng, H.; Zhang, J.; Guo, Y.; Sun, C.; Zhou, M.; Li, Q.; Ma, Z.; Ming, J. Quantitative Chemistry in Electrolyte Solvation Design for Aqueous Batteries. *ACS Energy Lett.* **2023**, *8* (2), 1076−1095.
(33) Cheng, H.; Sun, Q.; Li, L.; Zou, Y.; Wang, Y.; Cai, T.; Zhao, F.; Liu, G.; Ma, Z.; Wahyudi, W.; et al. Emerging Era of Electrolyte Solvation Structure and Interfacial Model in Batteries. *ACS Energy Lett.* **2022**, *7*, 490−513.
(34) Cai, T.; Wang, Y.; Zhao, F.; Ma, Z.; Kumar, P.; Xie, H.; Sun, C.; Wang, J.; Li, Q.; Guo, Y.; et al. Graphic, Quantitation, Visualization, Standardization, Digitization, and Intelligence of Electrolyte and Electrolyte-Electrode Interface. *Adv. Energy Mater.* **2024**, *14* (25), 2400569.
(35) Mariani, A.; Caminiti, R.; Ramondo, F.; Salvitti, G.; Mocci, F.; Gontrani, L. Inhomogeneity in Ethylammonium Nitrate-Acetonitrile Binary Mixtures: The Highest "Low q Excess" Reported to Date. *J. Phys. Chem. Lett.* **2017**, *8* (15), 3512−3522.
(36) Liu, X.; Mariani, A.; Zarrabeitia, M.; Di Pietro, M. E.; Dong, X.; Elia, G. A.; Mele, A.; Passerini, S. Effect of Organic Cations in Locally Concentrated Ionic Liquid Electrolytes on the Electrochemical Performance of Lithium Metal Batteries. *Energy Storage Mater.* **2022**, *44*, 370−378.
(37) Yoon, H.; Best, A. S.; Forsyth, M.; MacFarlane, D. R.; Howlett, P. C. Physical Properties of High Li-Ion Content N-Propyl-N-Methylpyrrolidinium Bis(Fluorosulfonyl)Imide Based Ionic Liquid Electrolytes. *Phys. Chem. Chem. Phys.* **2015**, *17* (6), 4656−4663.
(38) Grande, L.; Von Zamory, J.; Koch, S. L.; Kalhoff, J.; Paillard, E.; Passerini, S. Homogeneous Lithium Electrodeposition with Pyrrolidinium-Based Ionic Liquid Electrolytes. *ACS Appl. Mater. Interfaces* **2015**, *7* (10), 5950−5958.
(39) Pathirana, T.; Kerr, R.; Forsyth, M.; Howlett, P. C. Application of Super-Concentrated Phosphonium Based Ionic Liquid Electrolyte for Anode-Free Lithium Metal Batteries. *Sustain. Energy Fuels* **2021**, *5* (16), 4141−4152.
(40) Borodin, O.; Gorecki, W.; Smith, G. D.; Armand, M. Molecular Dynamics Simulation and Pulsed-Field Gradient NMR Studies of Bis(Fluorosulfonyl)Imide (FSI) and Bis[(Trifluoromethyl)Sulfonyl]-Imide (TFSI)-Based Ionic Liquids. *J. Phys. Chem. B* **2010**, *114* (20), 6786−6798.
(41) Tokuda, H.; Hayamizu, K.; Ishii, K.; Susan, M. A. B. H.; Watanabe, M. Physicochemical Properties and Structures of Room Temperature Ionic Liquids. 1. Variation of Anionic Species. *J. Phys. Chem. B* **2004**, *108* (42), 16593−16600.
(42) Liu, X.; Mariani, A.; Diemant, T.; Pietro, M. E. Di; Dong, X.; Kuenzel, M.; Mele, A.; Passerini, S. Difluorobenzene-Based Locally Concentrated Ionic Liquid Electrolyte Enabling Stable Cycling of Lithium Metal Batteries with Nickel-Rich Cathode. *Adv. Energy Mater.* **2022**, *12* (25), 2200862.
(43) Liu, X.; Mariani, A.; Diemant, T.; Di Pietro, M. E.; Dong, X.; Mele, A.; Passerini, S. Reinforcing the Electrode/Electrolyte Interphases of Lithium Metal Batteries Employing Locally Concentrated Ionic Liquid Electrolytes. *Adv. Mater.* **2024**, *36*, 2309062.
(44) Jiang, Z.; Zeng, Z.; Liang, X.; Yang, L.; Hu, W.; Zhang, C.; Han, Z.; Feng, J.; Xie, J. Fluorobenzene, A Low-Density, Economical, and Bifunctional Hydrocarbon Cosolvent for Practical Lithium Metal Batteries. *Adv. Funct. Mater.* **2021**, *31* (1), 2005991.
(45) Yoo, D. J.; Yang, S.; Kim, K. J.; Choi, J. W. Fluorinated Aromatic Diluent for High-Performance Lithium Metal Batteries. *Angew. Chem. Int. Ed.* **2020**, *59* (35), 14869−14876.
(46) Moon, J.; Kim, D. O.; Bekaert, L.; Song, M.; Chung, J.; Lee, D.; Hubin, A.; Lim, J. Non-Fluorinated Non-Solvating Cosolvent Enabling Superior Performance of Lithium Metal Negative Electrode Battery. *Nat. Commun.* **2022**, *13* (1), 4538.
(47) Tu, H.; Li, L.; Wang, Z.; Wang, J.; Lin, H.; Wang, M.; Yan, C.; Liu, M. Tailoring Electrolyte Solvation for LiF-Rich Solid Electrolyte Interphase toward a Stable Li Anode. *ACS Nano* **2022**, *16* (10), 16898−16908.
(48) Wang, Z.; Zhang, F.; Sun, Y.; Zheng, L.; Shen, Y.; Fu, D.; Li, W.; Pan, A.; Wang, L.; Xu, J.; et al. Intrinsically Nonflammable Ionic Liquid-Based Localized Highly Concentrated Electrolytes Enable

High-Performance Li-Metal Batteries. *Adv. Energy Mater.* **2021**, *11* (17), 2003752.
(49) Cai, Y.; Hou, Y.; Lu, Y.; Zhang, Q.; Yan, Z.; Chen, J. Ionic Liquid Electrolyte with Weak Solvating Molecule Regulation for Stable Li Deposition in High-Performance Li−O_2 Batteries. *Angew. Chem. Int. Ed.* **2023**, *62* (17), No. e202218014.
(50) Wan, H.; Xu, J.; Wang, C. Designing Electrolytes and Interphases for High-Energy Lithium Batteries. *Nat. Rev. Chem.* **2024**, *8* (1), 30−44.
(51) Chen, J.; Zhang, Y.; Lu, H.; Ding, J.; Wang, X.; Huang, Y.; Ma, H.; Wang, J. Electrolyte Solvation Chemistry to Construct an Anion-Tuned Interphase for Stable High-Temperature Lithium Metal Batteries. *eScience* **2023**, *3* (4), 100135.
(52) Begić, S.; Jónsson, E.; Chen, F.; Forsyth, M. Molecular Dynamics Simulations of Pyrrolidinium and Imidazolium Ionic Liquids at Graphene Interfaces. *Phys. Chem. Chem. Phys.* **2017**, *19* (44), 30010−30020.
(53) Preibisch, Y.; Horsthemke, F.; Winter, M.; Nowak, S.; Best, A. S. Is the Cation Innocent? An Analytical Approach on the Cationic Decomposition Behavior of N-Butyl- N-Methylpyrrolidinium Bis-(Trifluoromethanesulfonyl)Imide in Contact with Lithium Metal. *Chem. Mater.* **2020**, *32* (6), 2389−2398.
(54) Cao, X.; Ren, X.; Zou, L.; Engelhard, M. H.; Huang, W.; Wang, H.; Matthews, B. E.; Lee, H.; Niu, C.; Arey, B. W.; et al. Monolithic Solid−Electrolyte Interphases Formed in Fluorinated Orthoformate-Based Electrolytes Minimize Li Depletion and Pulverization. *Nat. Energy* **2019**, *4* (9), 796−805.
(55) Cao, X.; Gao, P.; Ren, X.; Zou, L.; Engelhard, M. H.; Matthews, B. E.; Hu, J.; Niu, C.; Liu, D.; Arey, B. W.; et al. Effects of Fluorinated Solvents on Electrolyte Solvation Structures and Electrode/Electrolyte Interphases for Lithium Metal Batteries. *Proc. Natl. Acad. Sci. U. S. A.* **2021**, *118* (9), No. e2020357118.
(56) O'Toole, T. R.; Younathan, J. N.; Sullivan, B. P.; Meyer, T. J. 1,2-Difluorobenzene: A Relatively Inert and Noncoordinating Solvent for Electrochemical Studies on Transition-Metal Complexes. *Inorg. Chem.* **1989**, *28* (20), 3923−3926.
(57) Liu, M.; Li, X.; Zhai, B.; Zeng, Z.; Hu, W.; Lei, S.; Zhang, H.; Cheng, S.; Xie, J. Diluted High-Concentration Electrolyte Based on Phosphate for High-Performance Lithium-Metal Batteries. *Batteries Supercaps* **2022**, *5* (5), No. e202100407.
(58) Olschewski, M.; Gustus, R.; Höfft, O.; Lahiri, A.; Endres, F. Monochromatic X-Ray Photoelectron Spectroscopy Study of Three Different Ionic Liquids in Interaction with Lithium-Decorated Copper Surfaces. *J. Phys. Chem. C* **2017**, *121* (5), 2675−2682.
(59) Chen, Y.; Ma, Z.; Wang, Y.; Kumar, P.; Zhao, F.; Cai, T.; Cao, Z.; Cavallo, L.; Cheng, H.; Li, Q.; et al. Trace Ethylene Carbonate-Mediated Low-Concentration Ether-Based Electrolytes for High-Voltage Lithium Metal Batteries. *Energy Environ. Sci.* **2024**, *17* (15), 5613−5626.
(60) Huang, A.; Ma, Z.; Kumar, P.; Liang, H.; Cai, T.; Zhao, F.; Cao, Z.; Cavallo, L.; Li, Q.; Ming, J. Low-Temperature and Fast-Charging Lithium Metal Batteries Enabled by Solvent−Solvent Interaction Mediated Electrolyte. *Nano Lett.* **2024**, *24* (24), 7499−7507.
(61) Lee, S.; Su, L.; Mesnier, A.; Cui, Z.; Manthiram, A. Cracking vsSurface Reactivity in High-Nickel Cathodes for Lithium-Ion Batteries. *Joule* **2023**, *7* (11), 2430−2444.
(62) Gu, W.; Xue, G.; Dong, Q.; Yi, R.; Mao, Y.; Zheng, L.; Zhang, H.; Fan, X.; Shen, Y.; Chen, L. Trimethoxyboroxine as an Electrolyte Additive to Enhance the 4.5 V Cycling Performance of a Ni-Rich Layered Oxide Cathode. *eScience* **2022**, *2* (5), 486−493.
(63) Wu, F.; Fang, S.; Kuenzel, M.; Mullaliu, A.; Kim, J. K.; Gao, X.; Diemant, T.; Kim, G. T.; Passerini, S. Dual-Anion Ionic Liquid Electrolyte Enables Stable Ni-Rich Cathodes in Lithium-Metal Batteries. *Joule* **2021**, *5* (8), 2177−2194.
(64) Heist, A.; Lee, S.-H. Electrochemical Analysis of Factors Affecting the Kinetic Capabilities of an Ionic Liquid Electrolyte. *J. Electrochem. Soc.* **2019**, *166* (8), A1677−A1684.
(65) Miao, Q.; Solan, N.; Hyun, G.; Holoubek, J.; Liu, P. Electrolyte Engineering for Long-Life Li-SPAN Batteries. *ACS Energy Lett.* **2023**, *8* (11), 4818−4830.
(66) Park, J. W.; Ueno, K.; Tachikawa, N.; Dokko, K.; Watanabe, M. Ionic Liquid Electrolytes for Lithium-Sulfur Batteries. *J. Phys. Chem. C* **2013**, *117* (40), 20531−20541.
(67) Peng, Y.; Badam, R.; Jayakumar, T. P.; Wannapakdee, W.; Changtong, C.; Matsumi, N. Drastic Effect of Salt Concentration in Ionic Liquid on Performance of Lithium Sulfur Battery. *J. Electrochem. Soc.* **2022**, *169* (5), No. 050515.
(68) Wang, J.; Yang, J.; Xie, J.; Xu, N. A Novel Conductive Polymer-Sulfur Composite Cathode Material for Rechargeable Lithium Batteries. *Adv. Mater.* **2002**, *14* (13−14), 963−965.
(69) Shen, Z.; Zhang, W.; Mao, S.; Li, S.; Wang, X.; Lu, Y. Tailored Electrolytes Enabling Practical Lithium-Sulfur Full Batteries via Interfacial Protection. *ACS Energy Lett.* **2021**, *6* (8), 2673−2681.
(70) Lee, S.; Koo, B.; Kang, S.; Lee, H.; Lee, H. Hydrofluoroether-Assisted Dilution of Na-Ion Concentrated Ionic Liquid Electrolyte for Safe, Stable Cycling of High-Voltage Na-Metal Batteries. *Chem. Eng. J.* **2021**, *425*, 130612.
(71) Tu, J.; Song, W. L.; Lei, H.; Yu, Z.; Chen, L. L.; Wang, M.; Jiao, S. Nonaqueous Rechargeable Aluminum Batteries: Progresses, Challenges, and Perspectives. *Chem. Rev.* **2021**, *121* (8), 4903−4961.
(72) Elia, G. A.; Ducros, J. B.; Sotta, D.; Delhorbe, V.; Brun, A.; Marquardt, K.; Hahn, R. Polyacrylonitrile Separator for High-Performance Aluminum Batteries with Improved Interface Stability. *ACS Appl. Mater. Interfaces* **2017**, *9* (44), 38381−38389.
(73) Xu, C.; Diemant, T.; Liu, X.; Passerini, S. Locally Concentrated Deep Eutectic Liquids Electrolytes for Low-Polarization Aluminum Metal Batteries. *Adv. Mater.* **2024**, *36* (24), 2400263.

https://doi.org/10.1021/acs.accounts.4c00653
Acc. Chem. Res. 2025, 58, 354−365